Chapter 5

Thermodynamically Stable Organic Inorganic Hybrid for Drug delivery vehicle to Shrinkage the Melanoma.

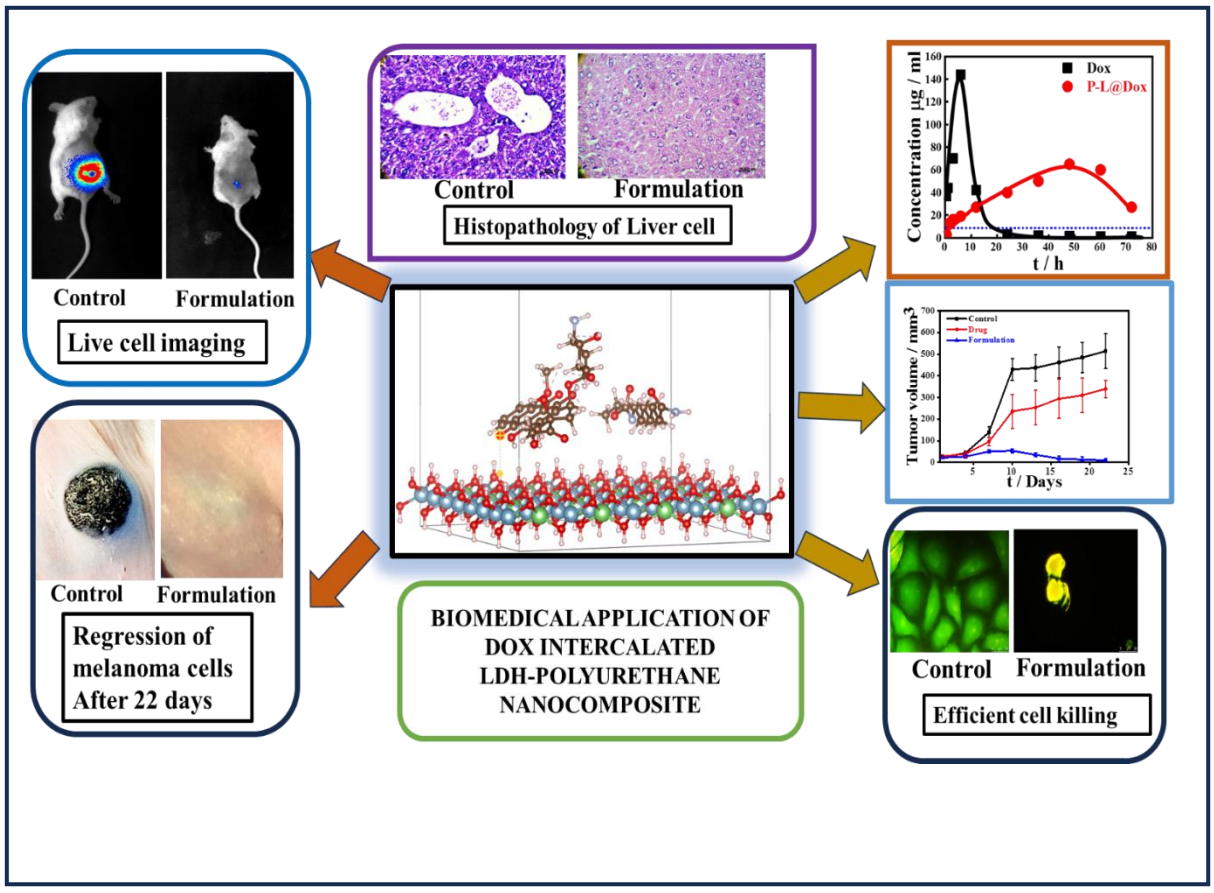

5.1 Introduction

In this evolving landscape, the focus lies on the development of novel, chemically linked, biocompatible graft copolymers tailored for sustained drug delivery, opening doors to innovative and effective therapeutic solutions.. The advancement of tumor treatment hinges not only on the development of biocompatible organic-inorganic hybrid but also on the discovery and application of therapeutic pathways that prove effective in clinical settings. Among these, apoptosis-based mechanisms have emerged as primary therapeutic targets in contemporary cancer therapies. A prime example is doxorubicin (Dox), a widely used antitumor antibiotic, which induces apoptosis in tumor cells through two key pathways: first, by integrating into the cancer cell's DNA and inhibiting topoisomerase II-mediated DNA replication; and second, by affecting mitochondrial function to form a semiquinone radical, thereby accelerating mitochondrial-driven apoptosis. Dox has shown great potential for expanding the arsenal of anticancer therapies, especially when combined with other treatment strategies. By exploiting these cell-destructive pathways, doxorubicin has demonstrated significant clinical efficacy against various forms of cancer, offering hope for the development of even more innovative cancer treatments [1]. In this study, the design of polyurethane-grafted inorganic Li-Al based LDHs is presented, carefully crafted to balance, followed by the incorporation of Doxorubicin (DOX) through ion-exchange techniques exploring their potential as a novel drug delivery system for the controlled release of the anticancer agent. Density Functional Theory (DFT) was utilized to explore the interaction dynamics and structural properties of Dox and prepolymer with LDH matrices along with integrating cutting-edge technologies - including machine learning, artificial intelligence (AI) - into the fabric of drug delivery, creating a seamless fusion of science and technology for future healthcare solutions. These grafted were meticulously characterized using various spectroscopic techniques to confirm their unique architecture

and the interactions between the organic - inorganic hybrid and drug molecules. Mechanical and thermal stability assessments were carried out to determine their practical applications. The antitumor efficacy and toxicity of these Dox intercalated prepolymer grafted LDHs were rigorously evaluated through *in vitro* and *in vivo* drug release profiles, contrasting their performance with that of free Dox. Experiments were conducted to elucidate the link between the observed antiproliferative effects and apoptotic signalling within the cells. The apoptotic mechanism was further examined via protein expression analysis using western blotting along with different biological techniques. This novel nanoformulation was also tested *in vivo* on melanoma-bearing mice, demonstrating significant tumor growth suppression, while ensuring no notable adverse effects on vital organs [2]. In this evolving landscape, the focus lies on the development of novel, chemically linked, biocompatible graft copolymers tailored for sustained drug delivery, opening doors to innovative and effective therapeutic solutions.

5.2. Result and discussion

5.2.1 Biocompatibility and *In Vitro* Cell Killing Efficiency of Dox-Loaded Nanovehicles:

Biocompatibility is a fundamental criterion in developing drug delivery systems and is typically evaluated through in vitro cell viability assays. In this study, a nanovehicle designed for efficient drug delivery in tumor treatment was assessed. The viability of SiHa cells exposed to the nanocomposite and its drug-loaded formulations was measured using the MTT assay over various time points. The MTT assay, which depends on the activity of NADPH enzymes in living cells, converts the MTT reagent into purple formazan crystals. Results indicated that the Li-Al-based LDH nanocarriers and their nanocomposite maintained nearly 100% cell viability after 72 hours of incubation, confirming their

suitability as biomaterials for drug delivery and other biological applications. Fluorescence imaging of cells treated with the nanovehicles (L, P, and P-L) shown in **Figure 5.1.a** revealed higher cell density and enhanced proliferation rates, emphasizing their excellent biocompatibility. Optical density measurements further supported the biocompatibility of all carriers (**Figure 5.1.b, c, e)**.

To evaluate the efficacy of the drug-loaded formulations, SiHa cells were treated with Dox-loaded materials (P@Dox and P-L@Dox). Fluorescence images of cells stained with acridine orange (AO) and ethidium bromide (EtBr) illustrated the cell death process, distinguishing between live and apoptotic cells. AO stains live cells green by binding to DNA, while EtBr selectively enters apoptotic cells, staining them red. Under AO/EtBr staining, apoptotic and necrotic cells emitted yellow-orange and red fluorescence, respectively, while healthy cells appeared green. Both Dox and P@Dox exhibited a mixture of live and apoptotic cells, whereas P-L@Dox showed a higher ratio of apoptotic cells, reflecting its potent antitumor activity -corroborated by MTT assay results over time **(Figure 5.2.b).**

The capability of these nanocarriers to release drugs in a controlled manner was assessed by comparing their cancer cell-killing efficiency. P@Dox and P-L@Dox formulations (20 µg/ml) achieved cell death rates of 67% and 95% in SiHa cells **(Figure 5.2.a)**, respectively, while the pristine drug (Dox) resulted in only 37% cell death (at pH ~7.4-8.0). The negatively charged Dox molecules faced challenges in efficiently penetrating the cell membrane due to electrostatic repulsion. However, the positively charged Dox-loaded grafted LDH nanocomposite successfully entered the cells, inducing apoptosis and necrosis. Over time**,** the Dox-loaded grafted LDH nanocomposite consistently reduced cell viability, with P-L@Dox demonstrating the highest cytotoxicity due to its sustained drug

release and enhanced uptake. This characteristic of P-L@Dox alleviates the need for frequent dosing, a common limitation associated with conventional delivery systems and pure drugs. The limited efficacy of pristine Dox can be attributed to its inability to maintain effective concentrations over time. To evaluate the toxicity of these nanovehicles, fibroblast cells (3T3-L1) were examined to assess their impact on normal, non-cancerous cells. All nanocarriers (L, P, and P-L) exhibited approximately 100% cell viability, confirming their non-toxicity and biocompatibility. In contrast, after 72 hours of incubation, Dox, L@Dox, P@Dox, and P-L@Dox displayed cell viabilities of 50±1.5%, 57±1.6%, 44±1.6%, and 70±1.2%, respectively **(Figure 5.2.c),** indicating significantly lower toxicity toward normal cells compared to cancer cells (SiHa). This suggests a degree of specificity for tumor cells, with P-L@Dox being more effective in targeting cancer cells while sparing normal ones.

\

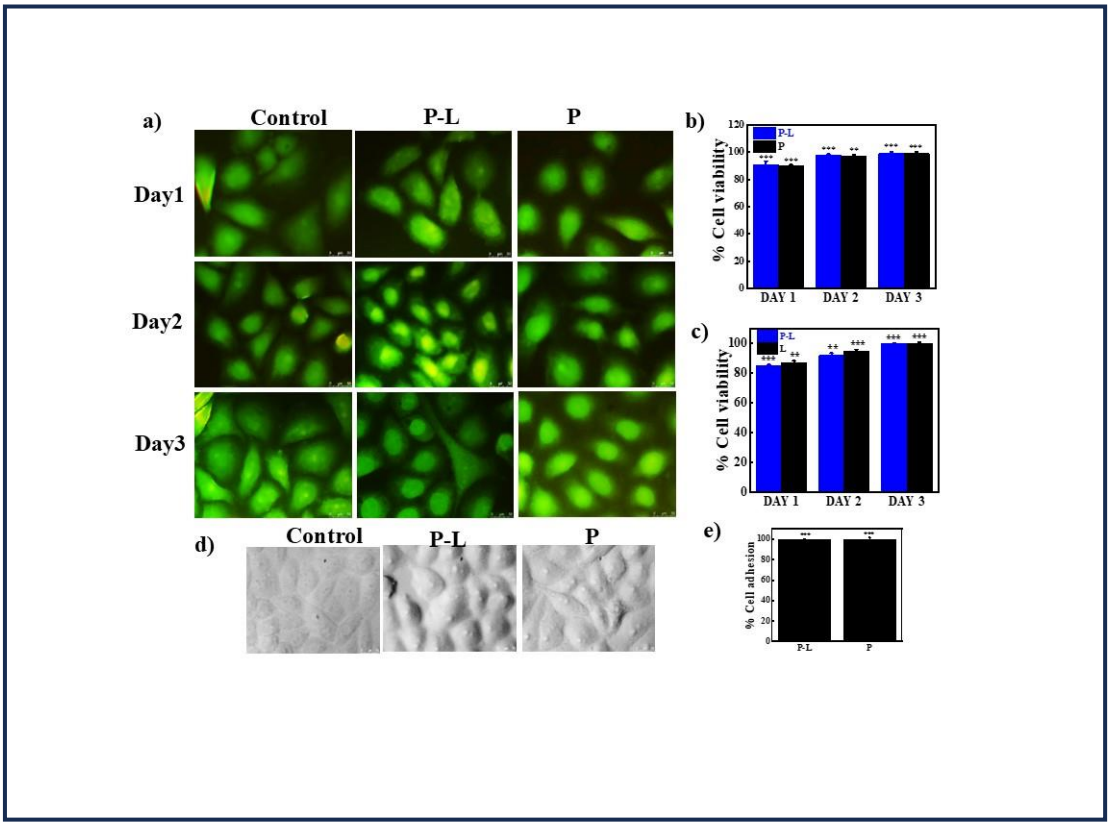

Figure 5.1 : a) Fluorescent microscopic images of AO/ EtBr staining of Control, P-L and P ; **b)** Cell viability study of Control, P-L and P against SiHa cells using MTT assay as a function of time; **c)** Cell viability of Control, P-L and P against 3T3-L1 using MTT assay as a function of time **d)** Phase contrast images of Control, P-L and P ; **e)** Percentage cell adhesion value of Control, P-L and P .

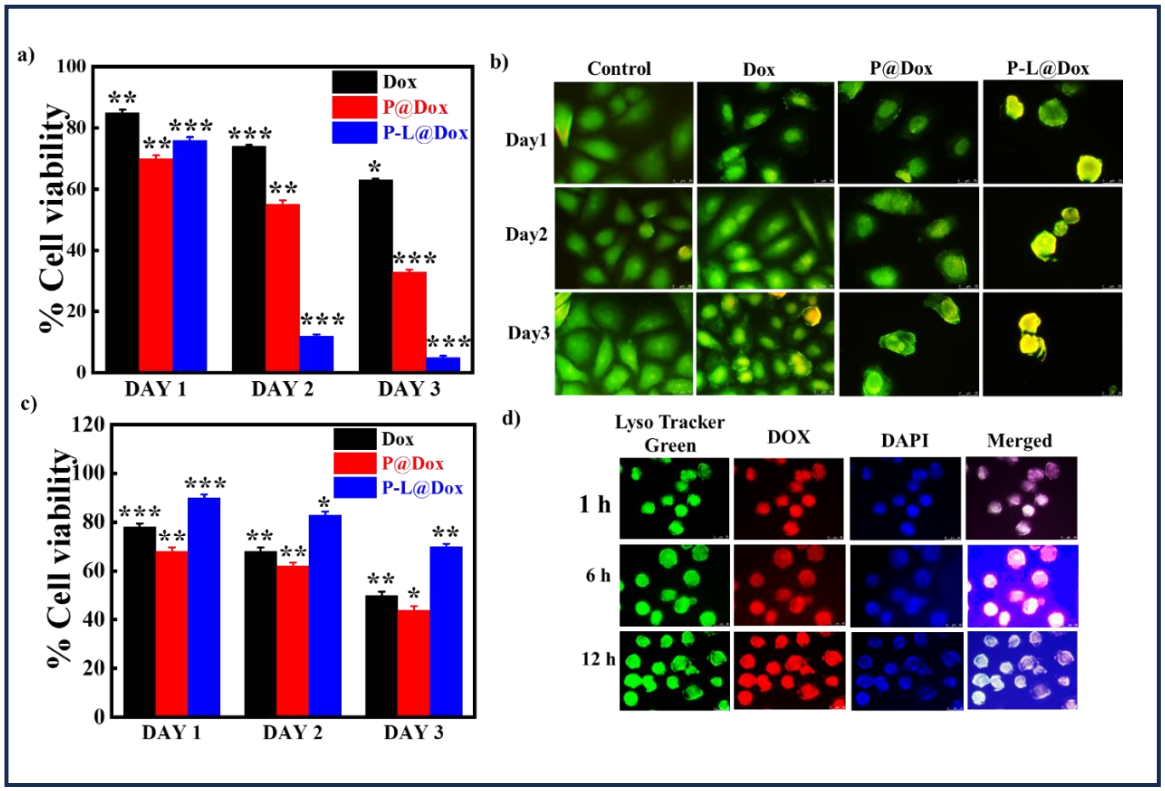

Figure 5.2: Comparative analysis of biocompatibility and *in vitro* cytotoxicity along with intracellular trafficking utilizing several trackers on the cancer cell line SiHa and the normal cell line 3T3-L1. **a)** MTT assay-based cell viability analysis of Dox, P@Dox and P-L@Dox against SiHa cells line at concentration 20 µg/ml; **b)** Fluorescence microscopy images of AO/EtBr staining of control, doxorubicin (Dox, pH~7-8), P@Dox and P-L@Dox at a concentration of 20 µg/ml reveal the relative number density of cells after treatment. **Scale bar: 50 µm and magnification:40x**; **c)** *In vitro* cytotoxicity of Dox, P@Dox and P-L@Dox groups (20 µg/ml) in 3T3-L1 fibroblast cells at different incubation time intervals:

results are shown in mean value ±SD, n = 3, *** $p < 0.001$, ** $p < 0.01$, * $p < 0.05$; and **d)** Microscopic images of SiHa cells that have been stained with 100 nM LysoTracker green and 5 µg/ml DAPI after being exposed to P-L@Dox in different time periods, **Scale bar: 50 µm and magnification:40x.**

Further investigation into the intracellular trafficking of P-L@Dox revealed that the nanoformulation entered SiHa cells via clathrin-mediated endocytosis. Initially, Dox localized within lysosomes, as demonstrated by colocalization with LysoTracker Green-labeled lysosomes after one hour of treatment (**Fig. 5.2.d**). However, as incubation time increased (1 h, 6 h, and 12 h), Dox progressively migrated to the nucleus, where it exerted its cytotoxic effects. These findings illustrate that P-L@Dox is effectively internalized, responds to the acidic environment of lysosomes, and releases its drug payload in the nucleus to induce cell death.

5.2.2 Understanding Controlled Cellular Uptake and Novel Nanocomposite-Induced Cell Adhesion:

To comprehend the impact of biologically active molecules on cells, it's crucial to understand how these molecules penetrate the cell membrane, transitioning from the extracellular environment into the cytoplasm. The effectiveness of drug molecules in eliminating cells relies heavily on their ability to cross the cell membrane from their delivery vehicles into the target cells. This study utilizes doxorubicin (Dox) loaded into polyurethane and nanocomposites, which exhibit anti-cancer properties, to compare the efficacy of drug uptake against pristine Dox used in conventional therapies.

Cellular uptake studies were conducted using the human cervical cancer cell line SiHa to investigate the biological effectiveness of the P@Dox and P-L@Dox formulations over

time (Fig. 4a). Fluorescence imaging revealed significant cellular uptake for both formulations, while the uptake of pristine Dox was markedly low. Notably, P@Dox showed rapid initial uptake, but this decreased over time, likely due to a burst release of the drug. In contrast, P-L@Dox exhibited sustained uptake that aligned with its corresponding drug release profiles. **(Figure 5.3.a)**

Time-dependent relative uptake, indicated by mean fluorescence intensity , illustrated a steady increase in uptake for the formulations, whereas pure Dox demonstrated minimal uptake over the same duration. It's important to note that pristine Dox, being negatively charged, encounters challenges in penetrating the cell membrane. In contrast, Dox embedded within the positively charged grafted LDH nanocomposite can more readily cross the membrane, leading to greater cellular uptake**. (Figure 5.3.b)**

Choy et al. demonstrated that Clathrin-mediated endocytosis plays a vital role in the uptake of the grafted LDH nanocomposite, which can accommodate dimensions up to 200 nm, ensuring adequate cellular uptake to transport Dox into the cell. Understanding the cellular absorption of the nanocomposite and Dox-loaded LDH nanocomposite involves two key processes: the initial adhesion of the nanocomposite to the cell membrane and subsequent interactions with lipids and proteins, which facilitate energy-dependent uptake.

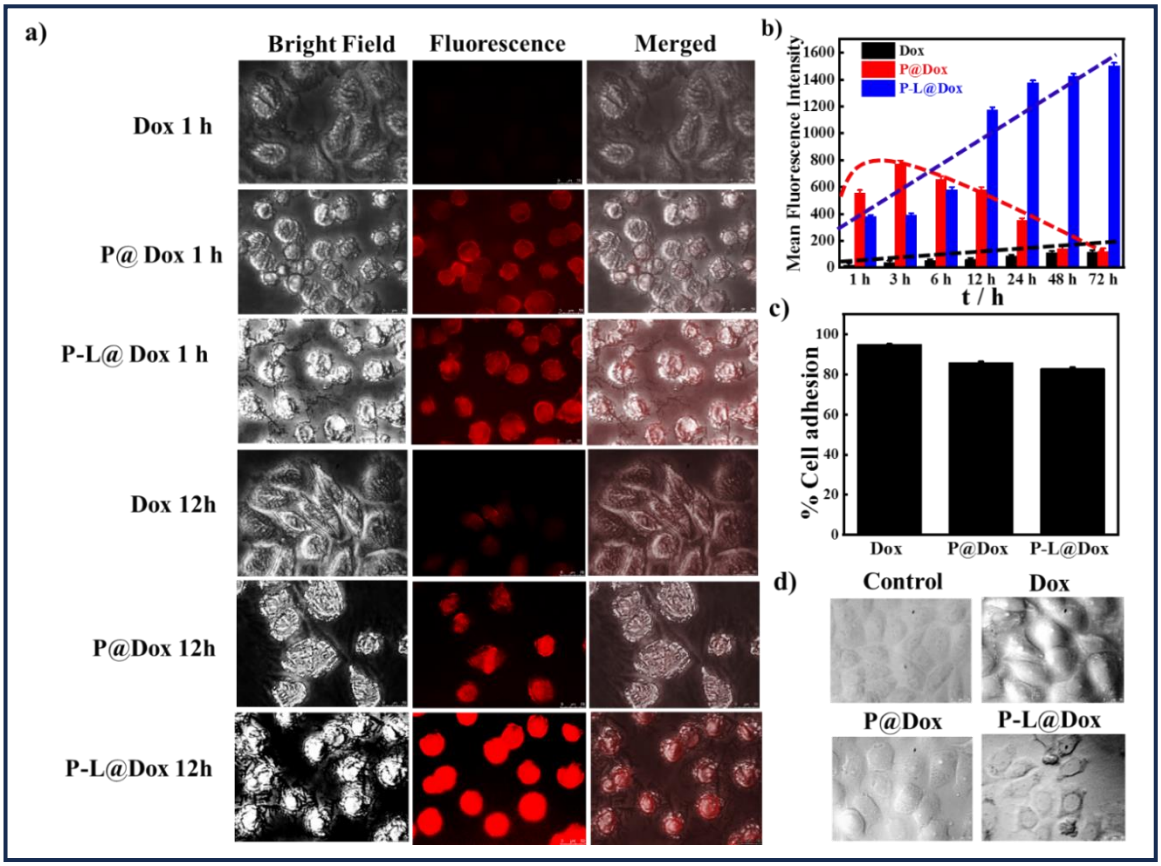

Figure 5.3: Dox-loaded prepolymer and prepolymer grafted Li-Al based LDH formulations: *in vitro* cellular characterization, capacity on uptake along with adhesion qualities in cancer cell line, SiHa. **a)** Fluorescence microscopy pictures showing the gradual uptake of Dox loaded P and L-P (P@Dox and P-L@Dox, respectively) by SiHa cells. Cells are subjected to 20 µg/ml Dox, P@Dox and P-L@Dox with different fluorescence intensities, depending on cellular absorption. **40x magnification and a 50 µm scale bar; b)** Analysis of the cellular uptake kinetics with SiHa cells under varied incubation times of P@Dox / P-L@Dox with equivalent Dox concentration of 20 µg/ml; **c)** The percentage cell adhesion values using the designed indicated nanoformulations after 24 hours of incubation for Dox was penetrated into the cells in the presence of P@Dox / P-L@Dox with equivalent Dox concentration of 20 µg/ml; **d)** Phase contrast images of the SiHa cells grown on the

indicated substrates after 24 hours of incubation, **40x magnification and a 50 μm scale bar** of P@Dox / P-L@Dox with equivalent Dox concentration of 20 μg/ml.

The effectiveness of material absorption correlates directly with its cellular adherence, a crucial factor in assessing the biocompatibility of a material. Cells must first attach to a substrate before they can proliferate. The polyurethane grafted Li-Al-based LDH nanocomposite and its formulations were evaluated qualitatively by examining morphological characteristics and quantitatively by measuring optical density to assess the viability of adhered cells. The cell morphology on the nanovehicles (P and P-L) without drug treatment displayed a flat, well-spread, and elongated shape with robust cell-to-cell connections (**Figure 5.3.d.),** indicating high biocompatibility. The adhesion percentages for P and P-L nanocomposites were 98±1.7% and 100±0.5%, respectively. In contrast, P@Dox and P-L@Dox showed a compressed morphology with reduced intercellular contacts due to the cytotoxic effects of Dox (**Figure.5.3.c),** resulting in viable cell percentages of 86±0.5% and 83±0.6% after 24 hours of incubation, highlighting their potential as effective nanocarriers **(Figure. 5.3.d).** The superior cell adhesion of the nanovehicles likely stems from the balanced functionalization between the hydrophilicity of LDH and the hydrophobicity of polyurethane, allowing cells to spread across the surface. This facilitates significant cellular uptake as the drug-loaded nanocomposites enter the cytoplasm via endocytosis, enhancing cell-killing efficacy.

5.2.3. Unveiling the Apoptotic Mechanistic Pathway *in Vitro*: Harnessing Novel Formulation for Precision Therapy:

Nuclear condensation, a marked decrease in cell volume, plasma membrane blebbing, nuclear fragmentation, and the formation of a distinct 200 base pair DNA ladder due to the internucleosomal degradation of chromatin are all hallmark indicators of apoptosis—a

programmed form of cell death initiated by specific stimuli. Importantly, during apoptosis, membrane integrity and mitochondrial function remain intact until the later stages of the process. Both apoptosis and necrosis involve the loss of phospholipid asymmetry in the cell membrane, where phosphatidylserine, usually confined to the inner leaflet, translocate to the outer leaflet. At the onset of apoptosis, following nuclear condensation but before membrane integrity is compromised, phosphatidylserine is externalized. This characteristic serves as the basis for fluorescence-activated cell sorting (FACS) methods that differentiate between early and late apoptotic cells, as well as necrotic ones, based on changes in membrane integrity. Key reagents in these assays include Annexin V, a protein with a high affinity for phosphatidylserine, and Propidium iodide, a dye that is excluded from cells with intact membranes.

Apoptosis is a crucial growth-regulating mechanism that allows cells to undergo self-destruction in a controlled manner. Selectively inducing apoptosis in tumor cells is one of the fundamental strategies in cancer treatment. Apoptosis can occur at various stages - early or late - depending on the severity of the stimuli. In a recent study, the apoptotic response of SiHa human cervical cancer cells treated with the nanocomposite (P-L), formulation (P-L@Dox), and pristine drug (Dox) was evaluated using Annexin V/PI staining. The results indicated distinct populations of cells at early, late apoptotic, and necrotic stages. Both Dox and P-L@Dox initiated apoptosis; however, the distribution of cells in late apoptotic and necrotic stages revealed a noteworthy trend. The percentages of necrotic/late apoptotic cells were 20/9.7 for pristine Dox and 50.2/31.7 for P-L@Dox, respectively. This data indicates a clear increase in necrotic stages alongside late apoptotic stages when using P-L@Dox, highlighting its efficacy as a potent nanovehicle for cancer cell eradication through sustained drug release. In contrast, pristine Dox was more associated with healthy cells, underscoring the enhanced therapeutic effectiveness of the P-L@Dox nanoformulation.

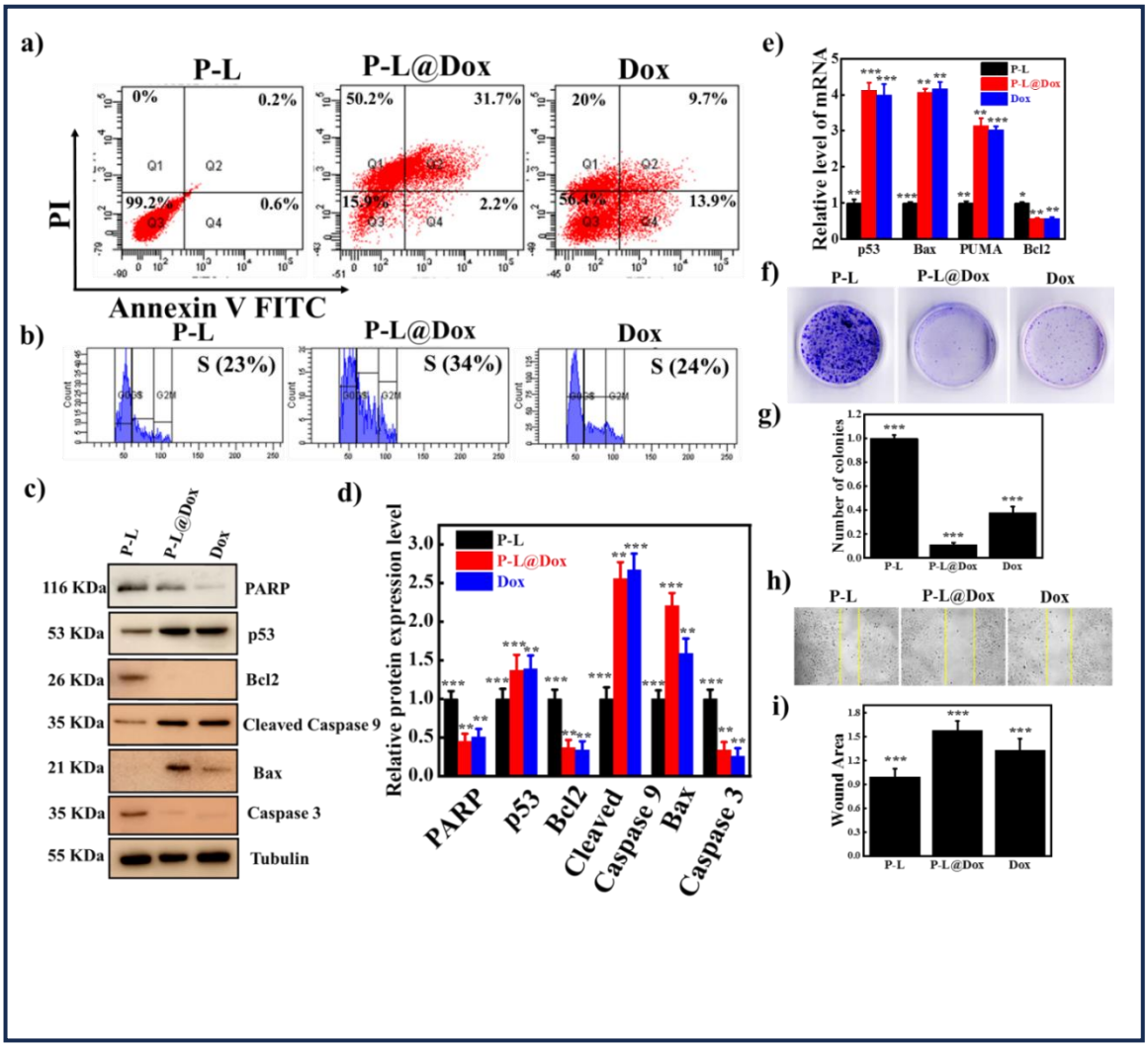

Fig 5.4. Assessment of the anticancer impact of the designed novel formulations (P-L@Dox) as compared to the traditional anticancer drug doxorubicin (Dox) for in vitro analysis. **a)** Using FACS study, the staining of SiHa cells exposed to P-L, Dox and P-L@Dox was evaluated for annexin V and propidium iodide. Cells were treated with designed nanocomposite and other two groups (20 µg/ml) for a 72 hrs. On the y-axis, the population tagged with propidium iodide (PI) is stained, and on the x-axis, Annexin V-FITC binding is visible. Necrotic and late apoptotic cells are located in the upper left (Q1) and right (Q2) quadrants, respectively; viable cells are found in the lower left (Q3) quadrant and are Annexin V negative and PI negative; early apoptotic cells are found in the lower right (Q4) quadrant and are Annexin V positive and PI negative; **b)** After being treated with

different chemotherapeutic drugs, cell cycles were stopped. SiHa cells were either treated with nanocomposite P-L, traditional anticancer drug Dox and designed formulation P-L@Dox (20 µg/ml) for a 72 hrs. To find DNA, the cells were fixed and stained with propidium iodide and the percentages of cells in the G0/G1, S, and G2/M states were calculated; **c)** SiHa cells were treated with 20 µg/ml of material (P-L), doxorubicin drug (Dox) and design formulation (P-L@Dox) for 72 hours. The expression of caspase 3, Bax, Cleaved caspase 9, Bcl2, p53, and PARP proteins were assessed by Western blot analysis; d) The relative expression of the specified protein markers has been meticulously quantified through western blot analysis; **e)** The relative expression levels of **mRNA** for **p53, Bax, PUMA**, and **Bcl-2** were quantitatively assessed through a detailed **RT-PCR** analysis; **f)** Photographic images of the colony study for Material, Dox, and P-L@Dox were captured after 72 hours of incubation for each sample, using a concentration of 20 µg/ml; **g)** Plot of number of colonies for material P-L, drug Dox and formulation P-L@Dox reflecting the potent efficacy towards cancer of the designed formulation; **h)** Microscopic images capturing the migration of SiHa cancer cells treated with material P-L, Doxorubicin Dox, and a specially designed formulation P-L@Dox after 72 hours incubation with samples concentration 20 µg/ml reveal striking evidence of enhanced efficacy. These images illustrate the profound impact of the treatment, showcasing a higher rate of apoptosis, as the cancer cells are visibly impaired in their movement, a testament to the potent therapeutic action of the formulation; **i)** The bar diagram illustrating the wound area across different groups such as, material P-L, Dox, and our designed formulation P-L@Dox elegantly reveals the potent efficacy of our novel formulation against cancer. The clear distinction between the groups highlights the remarkable impact of our formulation, emphasizing its therapeutic potential in comparison to the others.

FACS provides a refined and precise method for evaluating the potency and cell cycle specificity of anticancer agents like doxorubicin (Dox). This technique, which employs fluorescent vital stains, enables the rapid assessment of thousands of cells in viability tests. Additionally, cell cycle analysis using substances such as Propidium Iodide (PI)—which fluoresces upon intercalation with DNA—further enhances the accuracy of these evaluations. In a study with SiHa human cervical cancer cells treated with Dox and P-L@Dox at a concentration of 20 µg/ml, PI staining revealed a significant arrest in the S phase of the cell cycle. The results indicated that Dox and P-L@Dox induced apoptosis rates of 24% and 34%, respectively, demonstrating a clear dose-dependent effect on S phase arrest **(Figure. 5.4.a).** These findings provide quantitative insights into the mechanisms driving the apoptotic response and underscore the potential effectiveness of these drug formulations in targeting cancer cells.

Apoptosis, induced by anti-proliferative drugs, can occur via either the death receptor-dependent or mitochondrial-dependent pathways. A schematic representation of sustained drug delivery using an LDH-based nanoformulation, along with the biomolecular sequence leading to apoptosis (programmed cell death influenced by anticancer drugs), is presented in **Figure. 5.4.c.** Understanding the mechanisms of apoptosis within cells requires revealing the expression of specific apoptosis-related proteins. During the execution phase of apoptosis, the activation of caspases 3, 6, and 7, along with the cleavage of key cellular proteins, results in the characteristic morphology of apoptosis. Notably, the conversion of caspase 3 to its active form was significantly enhanced by Dox and P-L@Dox, showing fold changes of 0.26 and 0.34, respectively **(Figure. 5.4.d).** The detection of PARP cleavage in cells treated with P-L@Dox further supports caspase 3 activation, as PARP cleavage is a hallmark of apoptosis and a recognized target of caspase 3.

The Bcl2 family of proteins plays a critical role in regulating the intrinsic apoptotic pathway. The effectiveness of chemotherapy can be compromised when the anti-apoptotic protein Bcl2 is overexpressed. In this context, P-L@Dox appears more effective than Dox, as it reduces Bcl2 expression (fold changes of 0.34 vs. 0.37 for pure Dox). Our findings demonstrate that P-L@Dox treatment significantly lowers Bcl2 expression, suggesting that the intrinsic pathway is a key molecular mechanism in the apoptosis of SiHa cells induced by P-L@Dox. Cellular stress activates Bax, a tumor suppressor protein and sequence-specific transcription factor. Our experimental results indicate that the P-L@Dox formulation effectively arrests the S phase, as evidenced by the highest Bax expression levels compared to pure Dox and other formulations, with a fold change of 2.21 for P-L@Dox compared to 1.59 for Dox **(Figure. 5.4.d)**. Western Blot analysis reveals that the formulation induces a higher degree of apoptosis than the known drug. Cells treated with the formulation exhibit significantly increased expression of key pro-apoptotic proteins, including Bax, Puma, and p53 [3], compared to those treated with the drug, suggesting a more potent apoptotic response.

Overall, the results indicate that the formulation effectively drives apoptosis, with increased expression of pro-apoptotic markers and corresponding downregulation of anti-apoptotic markers. Thus, the developed P-L@Dox formulation demonstrates significant potential in modulating protein expression pathways for tumor treatment, supporting its application in future animal model studies.

The P-L@Dox formulation enhances the expression of pro-apoptotic genes at both the translational and transcriptional levels. As highlighted in the results section, cells treated with the formulation showed a significant upregulation in the transcript levels of p53 and PUMA compared to the known drug (Dox). Additionally, the transcript levels of the anti-

apoptotic gene Bcl2 were notably down regulated, reinforcing the findings of our Western blot analysis and providing strong support for the observed effects.

Cells treated with the P-L@Dox formulation exhibited significant suppression of growth and colony-forming potential, surpassing the effects seen with the known drug (Dox). This marked response serves as a strong indicator of enhanced apoptosis.

Furthermore, cell migration in response to treatment with either P-L@Dox or Dox was notably reduced compared to untreated controls. This suggests that both the formulation and the drug promote apoptosis, likely through the upregulation of p53 and other apoptotic proteins, thereby inhibiting cell migration [4]. Notably, migration was even lower in cells treated with the formulation than in those treated with the drug, underscoring the formulation's superior effectiveness in preventing tumorigenesis.

5.2.4. *In vivo* Tumor Treatment Using a Luciferase-Containing Melanoma Mouse Model with Pharmacokinetic Analysis:

The effectiveness of prolonged and sustained drug release was assessed in a mouse model with luciferase-expressing melanoma tumors through an innovative drug delivery method. Melanoma tumors measuring approximately 25 ± 5 mm^3 were established in mice using B16-F10 melanoma cells expressing luciferase. An injectable hydrogel was developed to tackle the challenges of drug delivery, ensuring prolonged contact with the tumor site after subcutaneous application. Methyl cellulose (MC) was selected as the gelling agent due to its biocompatibility and favourable gelation properties. At optimal concentrations, it forms an injectable gel, with its rheology extensively studied. Gelation behavior was assessed through the inversion tube test and *in vivo* methods.

The innovative treatment approach, as depicted in **Figure 5.5.a,** involved embedding the newly formulated nano-drug composite P-L@Dox within MC gel and injecting it directly beneath the tumor. This strategy was designed to utilize the enhanced permeability and retention effect for optimized melanoma treatment. Mice were divided into three groups, receiving saline (control), Dox in MC (Dox-MC), and the P-L@Dox formulation in MC (P-L@Dox-MC), with identical drug doses administered across all treatments. Remarkably, tumor volume decreased significantly over time in the P-L@Dox-MC treated group, reaching a measured tumor volume of 10 mm^3 after 22 days (**Figure 5.5.b**), while the control group experienced a steady increase in tumor volume (measured at 1700 mm^3). These results highlight the sustained drug release from P-L@Dox-MC, which maintained therapeutic dose levels at the tumor site for a longer duration compared to Dox-MC. In contrast, the rapid burst release from Dox-MC led to quick diffusion into the bloodstream, reducing bioavailability and overall tumor inhibition, resulting in minimal tumor suppression in the Dox-MC group.

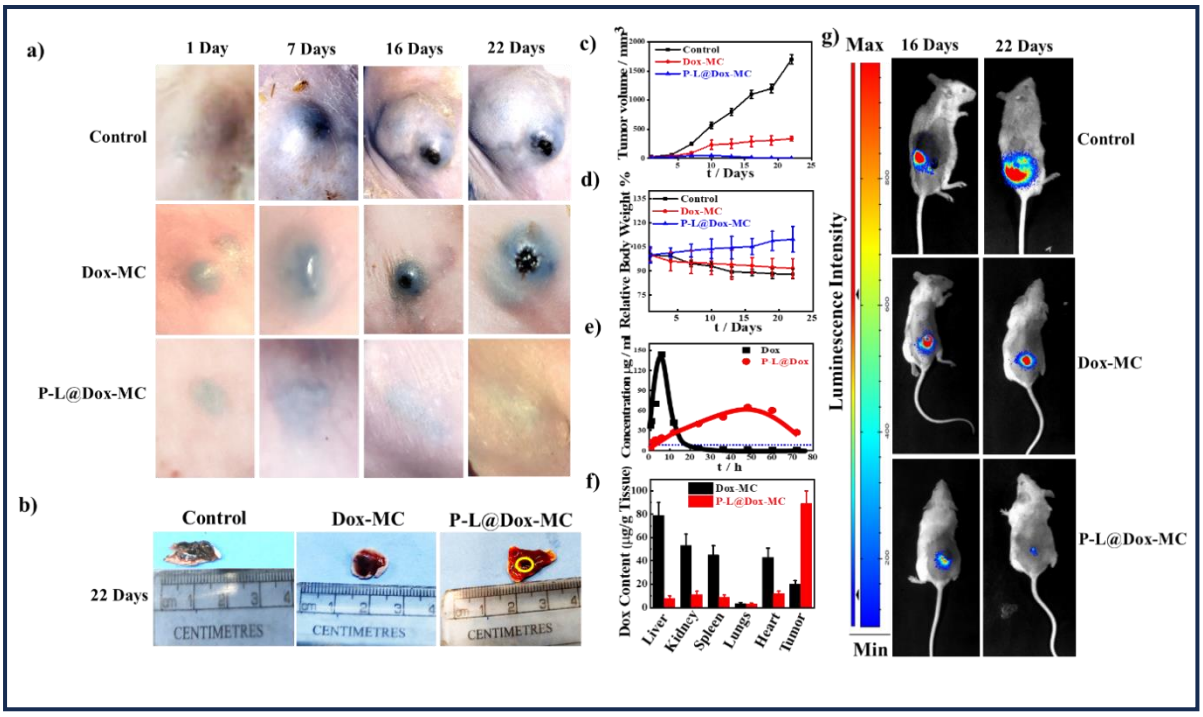

Figure 5.5: The effectiveness of the injectable formulation (P-L@Dox-MC) for in vivo therapy in mice with melanoma that contain luciferase. **a)** Images capturing the tumor sizes in mice, both before and after treatments, reveal the effects of various interventions. The treatments include Dox-MC (Dox encapsulated within an MC gel), P-L@Dox-MC (Dox incorporated into P-L, further embedded in an MC gel), and a control group receiving only saline. These visual comparisons offer a glimpse into the transformative impact of each treatment, providing a clear distinction between the progression or regression of tumors across the experiment; **b)** Photographic images showcasing the measured tumor volumes, accompanied by a scale, were captured after treatment across various groups i.e. Control, Dox-MC and P-L@Dox-MC. At the conclusion of the 22-day experiment, tumors from the different groups of animals were carefully collected and measured; **c)** Measured tumor volume over time as influenced by the therapy, with different approaches applied where appropriate, **d)** Percentage of relative body weight as a function of treatment time across all groups; **e)** After intravenous administration of either pure Dox (5 mg/kg of mouse body weight) or Dox intercalated within polyurethane prepolymer grafted Li-Al based LDH nanocomposite (P-L@Dox), containing an equivalent dose of the drug in dispersion form, the drug concentration profile in plasma was measured over time. The dotted line on the graph denotes the minimum inhibitory concentration (MIC) of DOX against *Mycobacterium smegmatis* (Msm); **f)** The levels of doxorubicin (Dox) in tumor tissue and various organs were assessed in melanoma tumor-bearing mice following treatment with Dox-MC and P-L@Dox-MC. This evaluation took place 72 hours after administering a dosage of 5 mg/kg; g) A Comprehensive study of bioluminescence in luciferase-expressing B16-F10 melanoma-bearing mice across three different groups over time.

The volume of tumors in the P-L@Dox-MC treated mice decreased to 340 mm^3, while those in the control and Dox-MC groups experienced significant weight loss due to severe side effects **(Figure. 5.4.d).** In contrast, the body weight of mice treated with P-L@Dox-MC increased steadily over time, indicating no adverse effects. The sustained release capability of P-L@Dox ensured that drug concentrations in the bloodstream remained within therapeutic levels for extended periods, thereby minimizing the side effects commonly associated with conventional Dox therapies. Analysis of blood concentrations following intravenous injection revealed that P-L@Dox provided a controlled release, maintaining concentrations above the minimum inhibitory concentration (MIC) for up to 70 hours. In comparison, the pristine Dox solution peaked early (Cmax = 144 μg/ml) and fell below the MIC within 15 hours **(Figure. 5.5.e).**

This study concluded that the larger, polyurethane-grafted Li-Al-based LDH nanocomposite serves as an ideal drug delivery vehicle. The accumulation of Dox in tumors treated with Dox-MC and P-L@Dox-MC was measured at 20 and 89 μg/g of tissue, respectively, demonstrating superior biodistribution in the P-L@Dox-MC group (Fig. 5.5.f). The higher concentration in tumors can be attributed to the positive surface charge of the nanocomposite, in contrast to the negatively charged pristine Dox. Furthermore, lower Dox concentrations were detected in vital organs such as the heart, liver, spleen, kidneys, and lungs in mice treated with P-L@Dox-MC compared to those treated with Dox-MC, significantly reducing the risk of organ toxicity. Notably, the elevated Dox levels in the liver of the Dox-MC group suggest a potential for severe side effects, further highlighting the safety and efficacy of the designed nanovehicle for melanoma treatment [5].

To evaluate the efficacy of the polyurethane-grafted Li-Al-based LDH nanocomposite P-L@Dox in reducing tumor size, we conducted qualitative analyses of tumor growth using bioluminescence imaging on the 16th and 22nd days of continuous treatment. This method relies on photon emission intensity resulting from the oxidation of D-luciferin in the presence of luciferase expressed by B16-F10 melanoma cells implanted in murine models. The results indicated a significant difference in luminescence intensity among the treatment groups, with the control group exhibiting the highest luminescence, followed by the drug-only group, and the formulation group demonstrating the lowest intensity. This luminescence intensity pattern - control > drug > formulation - correlates directly with the tumor volume growth curve, confirming the formulation's superior ability to inhibit melanoma cell growth. The formulation consistently displayed the weakest signal intensity, reinforcing its efficacy in targeting and killing malignant cells. Moreover, the distinct dynamics of the tumor growth curves align with the qualitative bioluminescence emission spectra, underscoring the therapeutic potential of the polyurethane-grafted Li-Al-based LDH nanocomposite P-L@Dox in melanoma treatment. These findings support the formulation's role in enhancing tumor suppression and suggest a promising avenue for further exploration in cancer therapeutics [6].

5.2.5. Histopathological and Immunohistopathological Analyses:

To understand the effects of controlled release on tumor treatment and to assess any potential adverse effects on vital organs, we performed a histopathological study to evaluate toxicity in key organs. Hematoxylin and eosin (H&E) staining was applied to critical tissues such as the liver, kidneys, spleen, lungs, and tumor sections collected post-treatment. In the control group, few necrotic regions with nuclear shrinkage were observed at the interface of the tumor (melanoma) and native connective tissue, showing minimal lymphocytic

infiltration and significant areas of necrosis **(Figure. 5.6.a).** In contrast, the group treated with the pristine drug (Dox-MC) exhibited mild to moderate lymphocytic infiltration and smaller areas of necrosis. Tumor tissue treated with the P-L@Dox-MC formulation showed a moderately dense collection of lymphocytes and large necrotic areas, indicating the formulation's potential to effectively target cancer cells.

The polyurethane-grafted Li-Al-based LDH nanocomposite demonstrated potent anti-tumor activity through a sustained-release mechanism, as supported by histological data. Additionally, mice treated with P-L@Dox-MC showed normal architecture in the liver and kidneys, with no signs of toxicity, unlike the control and Dox-MC groups, which displayed inflammation in the portal tract and deformations in hepatocyte shape and size **(Figure. 5.6.b).** The spleen and lungs across all groups remained free of noticeable damage. These findings suggest that the Dox-MC system may lead to severe side effects, likely due to the rapid release of the drug, which harms vital organs while providing minimal anti-tumor activity. In contrast, the developed P-L@Dox-MC formulation exhibited a slow and controlled release, maintaining therapeutic concentrations for longer periods. This controlled release enhances anti-tumor efficacy while preventing damage to vital organs. These advantages, resulting from sustained release, showing effective designed polyurethane grafted Li-Al based LDH nanocomposite,

preserve the drug’s bioavailability, leading to tumor shrinkage, improved melanoma inhibition, and overall better therapeutic outcomes without causing harmful side effects.

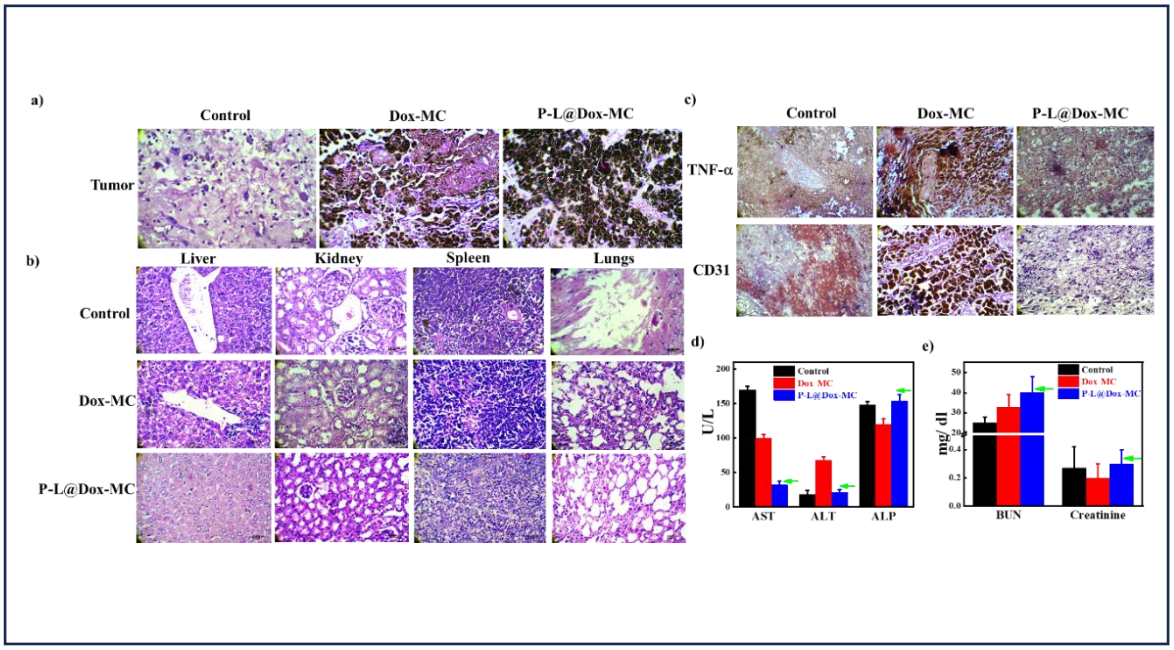

Figure 5.6: Examining the Complex Effects of *in vivo* Controlled Drug Release on Melanoma Tumor Tissues and Various Organs, Accompanied by Comprehensive Biochemical Assays a) Tumor tissues from mice across different treatment groups were carefully excised after 22 days of treatment and subjected to histopathological examination using H&E staining at a magnification of 40x.b) Following the same treatment duration, vital organs, including the liver, kidneys, spleen, and lungs, were collected from the mice and analyzed histopathological with H&E staining at 40x magnification. c) The immunohistochemical analysis of tumor tissues at the end of the treatment revealed detailed expressions of the inflammatory marker TNF-α and the vascular differentiation marker CD31, observed at a magnification of 40x.d) Liver function tests were conducted by analysing serum levels of AST, ALT, and ALP across different treatment groups, providing insights into hepatic health and functionality. e) Serum levels of BUN and creatinine were carefully assessed across the various therapy groups as part of a comprehensive renal

function test, with arrows indicating values corresponding to healthy mice as a benchmark for renal health.

Immunohistochemistry **(Fig. 5.5.c)** shows the expression levels of TNF-α and CD31 among all experimental groups. Notably, TNF-α expression was nearly absent in the P-L@Dox-MC group at the conclusion of the study, while it remained prominent in both the control and Dox groups. This suggests that inflammation subsides in the presence of P-L@Dox-MC, significantly enhancing angiogenesis and granulation compared to the other groups, thereby facilitating the healing process within the formulation group. Our findings provide compelling evidence that the drug-loaded nanocomposite embedded in the gel (P-L@Dox-MC) effectively accelerates tumor healing in mice [7].

Furthermore, the CD31 marker, which serves as a sensitive and specific indicator of vascular lesions, reflects the aggressive behavior of tumorigenic melanoma cells.[8] As shown in **Figure 5.6.c**, CD31 expression is significantly higher in the control and Dox groups, while it is completely absent in the P-L@Dox-MC group, indicating the potent efficacy of this formulation in melanoma treatment. Additionally, the stained images of melanoma treated with P-L@Dox-MC reveal substantial tumor cell death, far exceeding the results seen in the Dox-MC group.

To assess the safety of this treatment, liver and kidney function tests were performed. Key indicators of liver health, such as alanine aminotransferase (ALT) and aspartate aminotransferase (AST), remained within normal ranges for the P-L@Dox-MC group (ALT ~ 21 ± 4 U/L, AST ~ 32 ± 5 U/L), comparable to healthy mice (Fig. 9d). In contrast, mice treated with Dox-MC exhibited significantly elevated ALT (68 ± 5 U/L) and AST (100 ± 6 U/L) levels, suggesting severe liver damage after 22 days of treatment. These results strongly support the safety profile of P-L@Dox-MC in cancer therapy. Similarly, blood

urea nitrogen (BUN) and creatinine levels in the P-L@Dox-MC group were maintained within normal ranges (40 mg/dL and 0.3 mg/dL, respectively), while the Dox-MC group showed slightly lower values (33 mg/dL and 0.2 mg/dL), indicating renal distress **(Figure. 5.6. e).**

The fine-tuning of polyurethane grafting into Li-Al-based LDH nanocarriers resulted in a novel nanocomposite capable of encapsulating anti-cancer drugs, allowing for controlled drug uptake efficiency and sustained release properties. The unique architecture and various interactions of this carrier optimize drug delivery. Its superior biocompatibility and non-toxic behavior enhance anti-tumor activity without causing the severe side effects typically associated with conventional therapies. Therefore, this study demonstrates the promising potential of this nanocomposite as an effective drug delivery vehicle, particularly for cancer treatment.

5.3. Conclusion:

Hydrophilic inorganic Li-Al-based layered double hydroxide is elegantly grafted with organic hydrophobic polyurethane, creating an organic-inorganic nanocomposite hybrid with varied architectures to improve thermal stability and modify mechanical performance, achieving an extraordinary elongation at break of 1230%. This strategic modification facilitates a greater quantity of drug intercalation into the interlayer spacing of the LDH nanocomposite through ion exchange, resulting in sustained drug release. Spectroscopic analysis, coupled with DFT calculations, reveals marked peak shifts and decreases in energy, indicating strong binding between components. The minimum hydrogen-bonded distance further emphasizes this interaction.

Intercalating negatively charged doxorubicin into the nanocomposite matrix transforms the overall formulation into a neutral charged species, enhancing cellular uptake through the negatively charged cell membrane. The nanocomposite alone exhibits excellent biocompatibility, while the drug-embedded formulation demonstrates a remarkable 95% cancer cell-killing efficiency over three days. This stark contrast to the mere 37% efficiency observed with pristine doxorubicin can be attributed to significantly improve cellular uptake, as evidenced by fluorescence imaging. Fluorescence-activated cell sorting analysis further confirms the high apoptotic cell death induced by our designed formulation, in contrast to the predominantly healthy cells seen with pristine doxorubicin treatment.

The apoptotic mechanisms underlying these effects are revealed through the co-localization and expression of key proteins such as caspase 3, p53, and Bax, as shown by western blot analysis. Supporting the in vitro findings, in vivo studies on luciferase-expressing melanoma-bearing mice demonstrate a significant reduction in tumor volume when treated with the injectable hydrogel formulation. In contrast, only a modest reduction is observed with pristine doxorubicin under similar conditions. This enhanced efficacy is explained by the sustained release of the drug from the drug-loaded nanocomposite system compared to pure doxorubicin, further validated by biodistribution studies indicating higher doxorubicin concentrations in tumor tissue with the formulation.

Histopathological analyses reveal extensive tumor healing in mice treated with the designed formulation, while those treated with pristine doxorubicin show mild lymphocytic infiltration and limited necrosis. Additionally, the liver of mice treated with the novel formulation appears healthy post-treatment, whereas those treated with pristine doxorubicin exhibit inflammation in the portal tract and deformation of hepatocyte shape and size, underscoring the reduced side effects of the formulation compared to conventional

chemotherapy. Immunohistopathological studies corroborate the protein expression levels, aligning with the observed tumor healing.

In conclusion, this newly developed polyurethane-grafted Li-Al-based nanocomposite drug carrier offers a highly effective treatment for tumors, circumventing the adverse side effects typically associated with traditional anticancer therapies, and holds promise as a superior alternative in cancer treatment.

5.4. Reference

1) Thorn, C. F., Oshiro, C., Marsh, S., Hernandez-Boussard, T., McLeod, H., Klein, T. E., & Altman, R. B. (2011). Doxorubicin pathways: pharmacodynamics and adverse effects. *Pharmacogenetics and genomics*, *21*(7), 440-446.
2) Maity, S., Dubey, D. K., Meena, J., Shekher, A., Singh, R. S., & Maiti, P. (2024). Doxorubicin-Intercalated Li–Al-Based LDHs as Potential Drug Delivery Nanovehicle with pH-Responsive Therapeutic Cargo for Tumor Treatment. *ACS Biomaterials Science & Engineering*.
3) Klimentova, E. A., Suchkov, I. A., Egorov, A. A., & Kalinin, R. E. (2021). Apoptosis and Cell Proliferation Markers in Inflammatory-Fibroproliferative Diseases of the Vessel Wall (Review*). Sovremennye tekhnologii v meditsine*, 12(4), 119–126.
4) Wang, X., Decker, C. C., Zechner, L., Krstin, S., & Wink, M. (2019). In vitro wound healing of tumor cells: inhibition of cell migration by selected cytotoxic alkaloids. BMC pharmacology & toxicology, 20(1), 4.
5) Shukla, A., Singh, A. P., & Maiti, P. (2021). Injectable hydrogels of newly designed brush biopolymers as sustained drug-delivery vehicle for melanoma treatment. *Signal Transduction and Targeted Therapy*, *6*(1), 63.
6) Sônego, F., Bouccara, S., Pons, T., Lequeux, N., Danckaert, A., Tinevez, J. Y., ... & Tournebize, R. (2019). Imaging of red-shifted light from bioluminescent tumors using fluorescence by unbound excitation from luminescence. *Frontiers in bioengineering and biotechnology*, *7*, 73.
7) Shukla, A., Singh, A. P., Ray, B., Aswal, V., Kar, A. G., & Maiti, P. (2019). Efficacy of polyurethane graft on cyclodextrin to control drug release for tumor treatment. *Journal of colloid and interface science*, *534*, 215-227.

8) Pisacane, A. M., Picciotto, F., & Risio, M. (2007). CD31 and CD34 expression as immunohistochemical markers of endothelial transdifferentiation in human cutaneous melanoma. *Analytical Cellular Pathology, 29*(1), 59-66.